Structure–Function Spatial Covariance in the Human Visual Cortex

Mohammed K. Hasnain[1,2], Peter T. Fox[1–5] and Marty G. Woldorff[1,3]

[1]Research Imaging Center and Departments of [2]Physiology, [3]Radiology, [4]Medicine (Neurology) and [5]Psychiatry, The University of Texas Health Science Center at San Antonio, TX, USA

The value of sulcal landmarks for predicting functional areas was quantitatively examined. Medial occipital sulci were identified using anatomical magnetic resonance images to create individual cortical-surface models. Functional visual areas were identified using retinotopically organized visual stimuli, and positron emission tomography subtraction imaging with intra-subject averaging. Functional areas were assigned labels by placement along the cortical surface from V1. Structure-function spatial covariances between sulci and functional areas, and spatial covariances among functional areas, were determined by projecting sulcal landmarks and functional areas into a standardized stereotaxic space and computing the '*r*' statistics. A functional area was considered to spatially covary with a sulcus or another functional area if their geometric centers correlated significantly ($P < 0.05$) in two or more axes. Statistically significant spatial covariances were found for some, but not all comparisons. The finding of significant spatial covariances within a standardized stereotaxic space indicates that nine-parameter spatial normalization does not account for all the predictive value of structural or functional locations, and may be improved upon by using selected sulcal and functional landmarks. The present findings quantify for the first time the strength of structure–function spatial covariance and comment directly on developmental theories addressing the etiology of structure–function correspondence.

Introduction

The hypothesis of spatial covariance between sulcal anatomy and functional boundaries is based on the premise that the same developmental forces that shape the functional map, also give rise to the gross anatomical features of the brain. If a substantial spatial relationship between specific sulci and functional areas exists, then a useful prediction will be that a normalization technique incorporating sulcal landmarks will be better able to reduce intersubject variability of functional areas. This is important in physiological studies, because one would be able to determine with a greater degree of certainty as to where (in terms of functionality) one might be placing a probe in a normalized framework. The ability to better localize across individuals is also of paramount importance in neurosurgery and neurology, where highly visible sulci can greatly enhance the determination of functional boundaries.

Several developmental theories relating sulcation to the functional map have been put forward. These theories range from the theory of gyrogenesis as proposed by Welker (Welker, 1990), and the tension-based theory of morphogenesis by Van Essen *et al*. (Van Essen *et al*., 1997), on one hand, to the mechanical folding hypothesis by Richman *et al*. (Richman *et al*., 1975), on the other. These theories differ markedly in terms of the mechanisms involved, and the predictions that they make about sulcal–functional relationship. This is a rather profound reflection of the lack of consistent data on sulcal–functional relationships from which theories can be derived.

The value of quantitatively examining structure–function spatial covariance is twofold: (i) for testing the concept of using anatomical landmarks to improve on current spatial normalization techniques, and (ii) for evaluating theories of developmental relationships between structure and function. The present study reports the spatial covariance of early visual areas with respect to their neighboring sulcal landmarks in the occipital lobe, using the '*r*' statistic in a rather novel way.

Materials and Methods

Subject Population and Preparation

A total of 11 normal right-handed men, between the ages of 18 and 35 years, were recruited. A medical history battery questioned the subjects about neurological, psychiatric and cardiovascular history. Handedness restriction as assessed by history was used to avoid confounds due to differences in hemispheric anatomy between left- and right-handed subjects. Informed consent was obtained as approved by the institutional review board of the University of Texas Health Science Center at San Antonio.

Spatial Normalization

The bicommisural three-dimensional neuroanatomical coordinate space of Talairach and Tournoux (Talairach and Tournoux, 1988) is widely used as a standard stereotaxic reference system in which to report functional and anatomical data regarding the human brain. Individual brain images are normalized into Talairach space as follows. The brains are first translated and rotated to align the individual brain with the major axes of the Talairach space, defined by the midsagittal plane and the bicommisural line connecting the anterior and posterior commisures. The brains are then scaled in the three axes to match a standardized brain. The anterior commisure is considered as the origin in this reference space. The medial–lateral axis is referred to as the *x*-axis, the anterior–posterior axis as the *y*-axis, and the superior–inferior axis as the *z*-axis. Structures to the left of the midsagittal plane are assigned negative values along the *x*-axis, and those to the right of the midsagittal plane are assigned positive values, along the *x*-axis. Structures anterior to the anterior commisure are assigned positive values along the *y*-axis, whereas those posterior to the anterior commisure are assigned negative values along the *y*-axis. Similarly, areas superior to the bicommisural line connecting the anterior and posterior commisures are ascribed positive values along the *z*-axis, and those inferior to the bicommisural line are ascribed negative values along the *z*-axis. The power of this reference system lies in addressing brain anatomy in terms of Cartesian coordinates. Thus, a particular functional area or sulcal landmark can be reported to have a mean location and a variance about that location in *x*, *y* and *z* coordinates.

Anatomical Magnetic Resonance Imaging (MRI) Data Acquisition and Cortical Surface Modeling

To acquire the anatomical data, each of the subjects underwent a T_1-weighted MRI brain scan in a 1.9 T Elscint Prestige. A moldable plastic face-mask system was used to minimize motion during scanning. Anatomical images were obtained using a high-resolution, three-dimensional GRASS sequence: T_R = 33 ms; T_E = 12 ms; flip angle = 60°; voxel size = 1 mm^3; matrix size = 256 × 192 × 192; acquisition time = 15 min. The MRI data sets were normalized into Talairach space. Models

of the cortical surface, extending from the occipital pole to the parieto-occipital sulcus, were created for each subject from the MRI data sets. This was achieved by manually removing the scalp and the skull from the anatomic images, which were then modeled into continuous surfaces using the MRX software package (GE Research and Development Laboratory, Schenectady, NY). As the source MR images had been placed into Talairach space, the cortical surface models were also referenced within this space.

Experimental Tasks and Positron Emission Tomography (PET) Data Acquisition

Subjects were scanned under three experimental settings: fixation point (FIX), random dots along the horizontal meridian (HM), and random dots along the vertical meridian (VM). In the FIX (control) condition, subjects viewed a cross-hair with no other visual stimulation. In the HM and VM conditions, subjects viewed sectors of random-dots patterns refreshing at a rate of 8 Hz (Fox and Raichle, 1984). Each stimulation field extended from 1 out to 18 eccentricity, and spanned 60 of arc around the HM and VM respectively. Nine scans were acquired for the three test conditions in the sequence: FIX–HM–VM–FIX–VM–HM–FIX–HM–VM. In all instances but one, the entire protocol was completed satisfactorily. In that one subject, only two trials of the FIX condition were obtained due to cumulative radio-tracer dose constraints.

We employed functional PET (Hasnain *et al.*, 1998) rather than functional MRI to distinguish the visual areas, because this technique accurately and easily identified the borders between functional areas as local maxima in statistical parametric images. A GE/Scanditronix 4096 PET camera was employed: pixel spacing = 2.6 mm; spatial resolution = 5 mm FWHM (full-width at half-maximum) for events occurring within each emission scan; scan planes = 15; interplane, center-to-center distance = 6.5 mm; *z*-axis field of view = 10 cm. Events occurring in different emission scans were separable at a higher resolution (Fox *et al.*, 1986). This phenomenon is well known in signal detection theory as Vernier acuity (Lahti, 1965). Subjects were positioned in the PET scanner such that the plane of image acquisition was as perpendicular to the calcarine sulcus as possible. The same head restraint system as used in the MR imaging was employed for the PET scanner. PET data were acquired as regional distributions of tracer-associated radiation, using $H_2{}^{15}O$ (half-life, 123 s) as a freely diffusible blood-flow tracer, delivered via an intravenous bolus (Herscovitch *et al.*, 1983; Raichle *et al.*, 1983; Raichle, 1987). Arterial blood samples were not drawn, as the statistical significance and localization accuracy of functional mapping are not affected by compartmental modeling (Fox and Mintun, 1989). Each scanning session consisted of one transmission scan (used for attenuation correction), followed by nine emission scans (separated by 11 min intervals), three for each of the three conditions, as mentioned above. An emission scan was triggered by the arrival of the tracer bolus in the field of view of the camera, and images were acquired in two frames: a 40 s frame (stimulus-on) followed by a 50 s frame (stimulus-off).

PET Image Processing

Interscan head motions were removed by using a modified version of the AIR algorithm (Woods *et al.*, 1993). The PET images were also spatially transformed into the proportional bicommissural space, as defined by the Talairach–Tournoux atlas (Talairach and Tournoux, 1988), using the Lancaster algorithm (Lancaster *et al.*, 1995). The dimensions of a particular individual's brain along the three axes were derived from MRI data and the same scaling factors were used to normalize both functional and anatomical images into Talairach space. The resulting brain contours in the two data sets were co-registered within 2 mm (one pixel) of each other in each of the three axes. Images were value normalized by applying a one-parameter scale factor, setting the whole-brain mean value to an arbitrary value of 1000 (Fox *et al.*, 1984; Fox and Mintun, 1989). Following normalization, images were tri-linearly interpolated, resampled (60 slices, voxel size 8 mm^3) and filtered through a Gaussian filter, sized 3 × 3 × 3 voxels.

For each individual, the three repetitions of each condition were averaged. The three-image averages were then contrasted on a voxel-wise basis, creating per-subject statistical parametric images (SPI) of task-induced changes in regional blood flow for each of the two stimulus conditions (HM and VM), relative to the control state (FIX). For each SPI, an automated search for local maxima and minima was performed using a search volume measuring 27 mm^3 (Mintun *et al.*, 1989). Change distribution analysis (Fox *et al.*, 1988) was used to assess the statistical significance of the identified outliers. *Post-hoc* (regional) tests for statistical significance were performed by converting SPIs to *z*-score images, based on the variance of all local changes within each nine-image set for each subject. Images were then thresholded to a *z*-score cut-off of 2 ($P < 0.05$).

Functional Labeling of local maxima

Echoplanar fMRI studies (Sereno *et al.*,1995; DeYoe *et al.*,1996) have demonstrated the possibility of identifying extra-striate areas in the occipital lobe, using retinotopic stimuli with neuroimaging techniques. These studies were based on literature describing the retinotopic organization of pre-striate visual areas in non-human primates (Daniel and Whitteridge, 1961; Van Essen and Zeki, 1978; Newsome *et al.*, 1986; Gattass *et al.*, 1988; Felleman and Van Essen, 1991), and also on lesion analysis data describing visual field deficits in man (Holmes, 1945; Clarke and Miklossy, 1990; Horton and Hoyt, 1991a,b). Both the imaging and the lesion-analysis studies indicate that a retinotopic organization similar to that in the macaque exists in man, such that each of the visual areas V1, V2v, V2d, VP, V3 and V3a contains a more-or-less retinotopic map. These areas lay out on the cortical ribbon in a continuous manner, beginning with V1 and moving along a dorsal–ventral axis to V1. The visual areas border one another at their HM and VM representations. Thus, the meridian stimuli allow us to define the borders of functional areas, and the order of occurrence of these borders on the cortical surface establishes the identity of the visual areas.

Labeling of functional areas was performed by superimposition of regional activations as detected by PET-derived *z*-score images, on the surface models for the occipital lobes, and by following the cortical surface along a dorso-ventral axis from V1 HM representation. The cortical surface was followed using the MRX software package (GE R&D Laboratory), while being viewed in the three orthogonal dimensions, utilizing a customized three-dimensional visualization tool kit (Lancaster *et al.*, 1995). The calcarine sulcus has been established as the typical site of the HM representation in the primary visual cortex (V1) of man. Therefore, the HM activation in V1 [V1(H)] was identified by reference to the calcarine sulcus. Extrema showing positive blood flow changes were analyzed. All HM-condition extrema that formed a contiguous cluster of activation (*z*-score > 2) and were within 6 mm of the calcarine sulcus were included as part of V1(H). Following the cortical surface ventral to the calcarine sulcus, the next HM activation site was identified, and all extrema within this activated area were considered to be part of the V2v/VP border. Similarly, following the cortical surface dorsal to the calcarine sulcus, the HM activation site immediately dorsal to V1(H) was identified and all extrema contributing to this activation site were considered to be part of the V2d/V3 border. The extrema forming V1(H), the V2v/VP border and the V2d/V3 border were mutually exclusive. The above predefined criteria identified V1(H), V2v/VP and V2d/V3 in all but two right hemispheres, in which no HM activation lay within 6 mm of the calcarine sulcus. For these two cases, V1(H) was defined *post hoc* as the HM activation which lay closest to the calcarine. A *z*-score of 2.5 was used to raise specificity because V1(H) was frequently the most robust activation. Overlaid on the cortical surface this *post-hoc* analysis correctly identified V1(H) as the middle activation in a pattern of three horizontal meridian activations centered on and lying along a dorsal–ventral axis to the calcarine.

The VM representations were analyzed such that the VM activation site immediately ventral to V1(H) was labeled as the V1/V2v border. VM representation immediately ventral to the V1/V2v border was identified as the anterior border of area VP. Likewise, the VM activation site immediately dorsal to V1(H) was labeled as the V1/V2d border, and the next VM representation dorsal to the V1/V2d border was identified as the V3/V3a border.

Extrema coordinates within each visual area border were averaged together to yield the coordinates for the geometric center of that border. The coordinates for the geometric center of a particular visual area were obtained by averaging those for the area's borders, e.g. the center of V2v was obtained by averaging the coordinates for its borders V1/V2v and V2v/VP. Note that the above-mentioned functional areas were identified

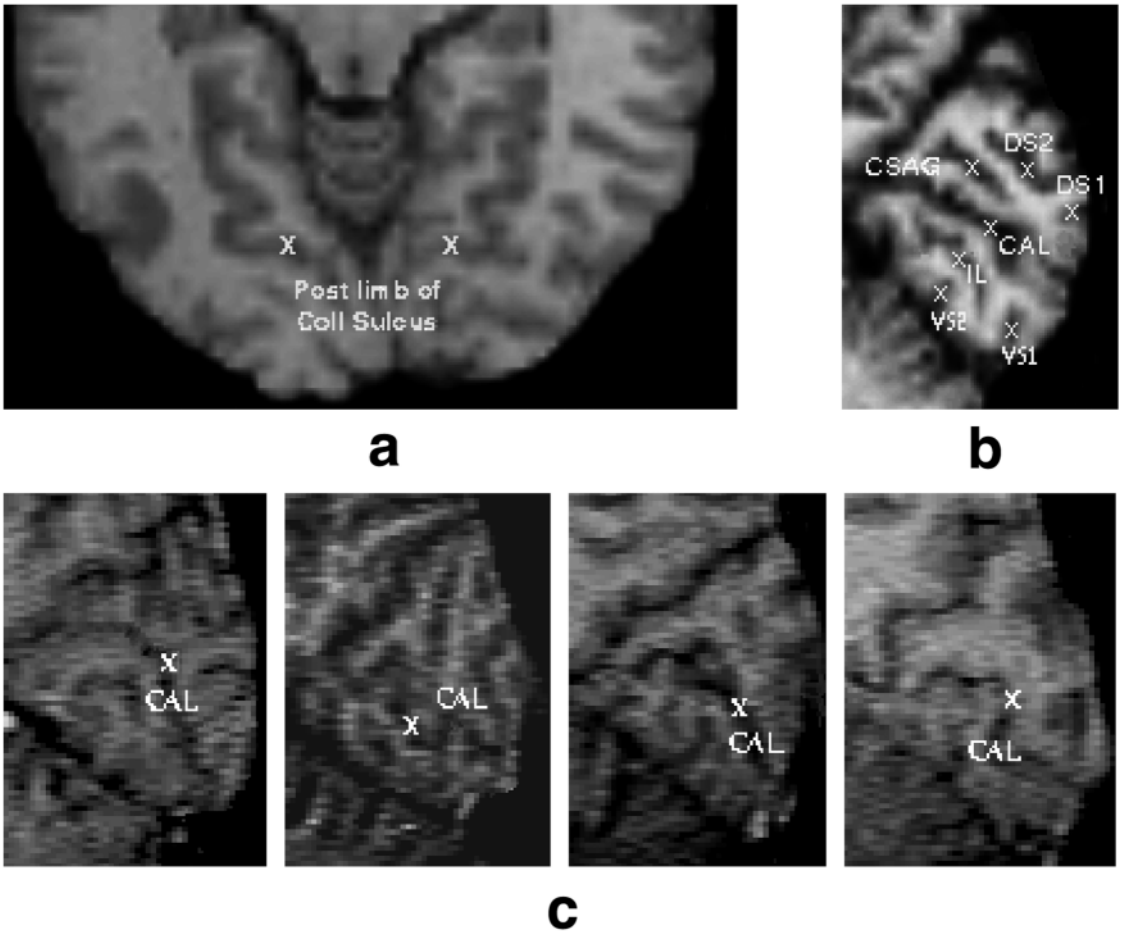

Figure 1. (*a*) Axial view of the brain showing the collateral sulcus (Coll). × marks the approximate center of the posterior limb of the collateral sulcus. (*b*) Sagittal MRI view of the brain illustrating relative locations of occipital sulci identified in the study. CAL, calcarine sulcus; DS1, first dorsal sulcus to the calcarine; DS2, second dorsal sulcus to the calcarine; VS1, first ventral sulcus to the calcarine; VS2, second ventral sulcus to the calcarine; IL, intralingual sulcus; CSAG, cuneosagittal sulcus. × marks the approximate center of a sulcus used in the correlation analysis. (*c*) Para-sagittal views of four hemispheres 8 mm from the midline, illustrating the variability in the shape of the calcarine sulcus.

without relying either on the secondary sulci or on previously reported Talairach coordinates.

For the 'color-sensitive' area (V4v) as identified by Zeki *et al*. (Zeki *et al.*, 1991), a directed local-maximum search strategy was performed because the retinotopy in this area is not well defined. The search was implemented within a fixed radius of 2 cm of the previously reported mean coordinates for area V4v as follows: a pair of HM and VM activation sites, each with a *z*-score > 2 ($P < 0.025$), separated by <10 mm (the reported dimensions for this area are approximately 15 × 15 mm), and lying closest to the mean coordinates previously reported (Zeki *et al.*, 1991) for area V4v, were identified. Except for the anterior VP border (which may be part of area V4v), responses identified as V1, V2v, V2d, V3 and V3a were excluded from this directed local-maximum search. The area was considered to have failed detection in an individual if no paired responses meeting the above criteria were found. This approach, first implemented by Fox and Pardo (Fox and Pardo, 1991), and a comparable approach used by Hunton *et al*. (Hunton *et al.*, 1996) in their analysis of functional–anatomical variability in neuroimaging studies, has been shown to resolve group activations that are not closely clustered.

Labeling of Occipital Sulci

Sulcal designations were based on order and orientation with respect to the calcarine sulcus as visualized on the cortical surface models. The calcarine sulcus was identified (Fig. 1), using two atlases (Ono *et al.*, 1990; Duvernoy, 1991) as guides. In all but one case (21 out of 22), the calcarine sulcus was easily defined as the only major sulcus extending from the occipital pole to the junction with the parieto-occipital sulcus. In the remaining one case there were two sulci that fitted the above criteria. In this particular case cross-validation from independent observers was sought to help determine which of the two sulci should be labeled as the calcarine. Starting from the occipital pole, the first and the second sulci immediately dorsal to the calcarine with their origins on the posterior surface of the brain were marked. These were labeled as 'the first dorsal sulcus' and 'the second dorsal sulcus' respectively. Similarly, starting from the occipital pole, the first and the second sulci immediately ventral to the calcarine with their origins on the inferior surface of the brain were identified, and labeled as 'the first ventral sulcus' and 'the second ventral sulcus' respectively. The collateral sulcus was also identified using the two atlases (Ono *et al.*, 1990; Duvernoy, 1991) as guides. This sulcus was usually the only sulcus starting from the inferior-medial surface of the occipital lobe and extending midway into the temporal lobe. Again, independent observers were asked to cross-validate when there was any doubt in designation. In cases where the posterior limb of the collateral sulcus also happened to be the first or the second ventral sulcus, the sulcus was given both designations and counted in the analysis for both sets of sulci. To avoid labeling the dorsal sulci twice, a sulcus immediately dorsal to the calcarine without extension to the posterior surface was named the cuneosagittal sulcus. Similarly, a sulcus immediately ventral to the calcarine without extension to the posterior surface was named the intralingual sulcus.

A concept similar to that of the center-of-mass of an activation in PET data was used to assign a reference value to a given sulcus in an individual. The length of each sulcus was determined using the cortical surface model. The point midway between the sulcal lip and the sulcal fundus, at

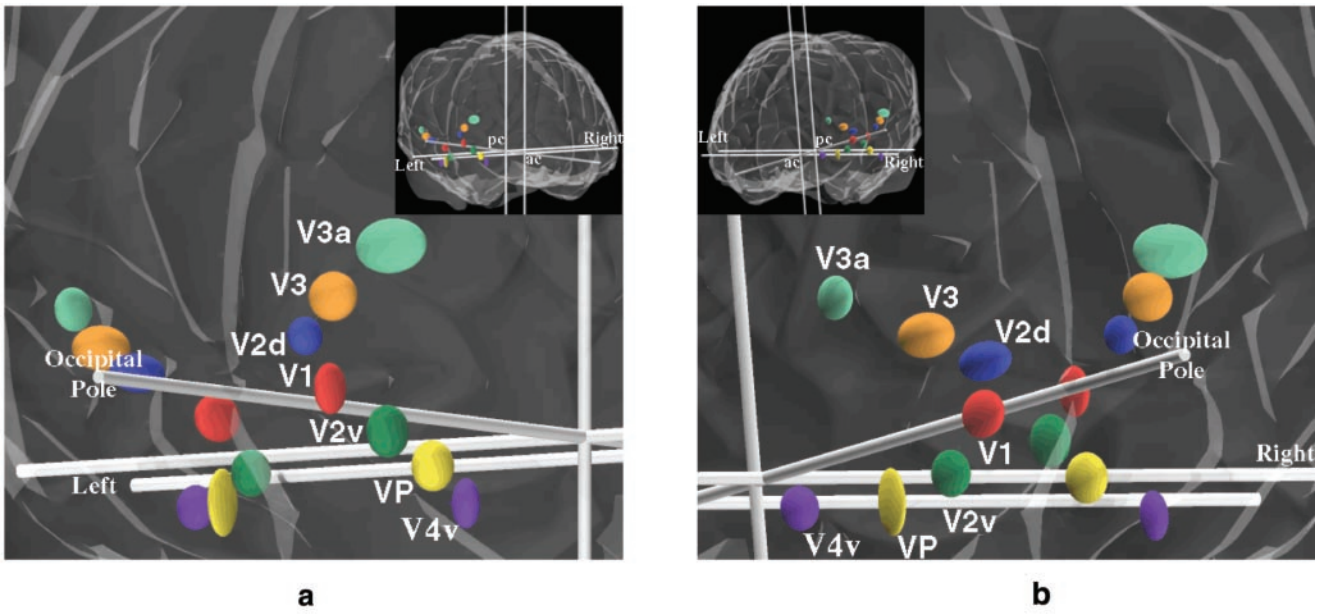

Figure 2. Right posterio-lateral (*a*), and left posterio-lateral (*b*) views of a brain model, using ellipsoids centered at the mean locations of the early visual areas in Talairach space. The radius of an ellipsoid in a particular axis represents the positive standard deviation of the area in that axis. ac, anterior commisure; pc, posterior commisure.

mid-length, was chosen as the center of the sulcus. This point was henceforth used as the reference point for that sulcus in correlation analysis. In case of the collateral sulcus, the center of its posterior limb was taken as the reference point.

Sulcal–Functional Spatial Covariances

The locations of functional areas for each of the subjects were overlaid onto the corresponding anatomical MR images and the sulcal landmark closest to a given area was identified. The center-to-center distance of a given area from the closest sulcal landmark was calculated in each subject. Pairwise correlation analysis was carried out for each area and sulcus within each hemisphere. An area was considered to significantly covary with a sulcus or another area only if the pair had positive spatial correlations with a $P < 0.05$ ($r = 0.6$ for a sample size of 11) in *at least two axes.*

The number of pairs examined, looking for covariance between seven functional areas, their borders and six sulci in each hemisphere, was 175 (k). Given the large number of multiple comparisons, we calculated the probability of making a type I error in our analysis. If we assume that any statistically significant correlations were due to chance alone, it follows that these *randomly* occurring 'significant' correlations in the three axes would be independent of each other. In such a case we can apply the multiplicative rule of probabilities, and the odds of a sulcus and a functional area having significant correlations in two of the three axes by chance alone (μ) is ~1 in 400 or $P < 0.0025$. Correcting for multiple comparisons, the probability of making a type I error at least once [$\alpha_T = 1 - (1 - \mu)^k$] in our analysis of 175 comparisons is 0.45 (a probability considered acceptable for large number of comparisons).

Table 1
Mean location and standard deviation of early visual areas

Area	Talairach coordinates						Frequency of detection (%)
	Mean location (mm)			Standard deviation (mm)			
	x	*y*	*z*	*x*	*y*	*z*	
Right hemisphere ($n = 11$)							
V1	6.2	–79.9	0.9	2.6	5.7	5.0	100
V2v	7.8	–71.1	–3.3	4.0	5.9	5.9	100
V2d	8.2	–87.6	6.1	3.5	4.3	4.5	100
VP	12.9	–69.7	–7.3	4.4	5.7	5.4	100
V3	12.0	–87.6	10.3	5.9	5.5	4.2	100
V3a	17.4	–84.1	15.9	9.3	6.1	3.4	91
V4v	19.4	–72.6	–12.0	3.3	5.6	2.9	100
Left hemisphere ($n = 11$)							
V1	–7.2	–82.5	–1.9	3.3	5.3	7.5	100
V2v	–7.7	–75.3	–7.5	4.2	5.1	4.9	100
V2d	–11.7	–91.5	2.7	4.6	4.3	8.6	91
VP	–13.7	–72.2	–10.2	2.0	7.6	5.1	100
V3	–17.9	–89.6	5.9	5.9	5.0	7.5	91
V3a	–25.7	–83.8	11.0	2.9	4.9	6.1	82
V4v	–21.8	–65.8	–9.9	4.5	5.0	3.6	100

x-axis = medial–lateral axis; positive values indicate location to the right, and negative values location to the left from the midsagittal plane, in millimeters. *y*-axis = anterior–posterior axis; positive values describe location anterior to, and negative values location posterior to the anterior commisure, in millimeters. *z*-axis = superior–inferior axis; positive values are location superior to, and negative values are locations inferior to the bicommisural line connecting the anterior commisure and the posterior commisures, in millimeters.

Results

Frequency of Observations

Functional Areas

The results of observations on the early visual functional areas in terms of their locations and locational variability in Talairach space are summarized in Table 1 (Fig. 2). Briefly, regions of activation alternating between those due to the HM stimulus and those due to the VM stimulus were observed extending outwards from the V1 HM representation [V1(H)]. This pattern of activation continued up to area V3a in the dorsal occipital cortex, and down to the anterior border of area VP in the ventral occipital cortex. The frequency of detection for a given area ranged between 82 and 100%.

Area V4v was usually found to be adjacent to area VP, but not always (Fig. 3). The mean distance between area V4v and the corresponding Zeki coordinates (Zeki *et al.*, 1991) was 5.2 mm in the left hemisphere, and 10.4 mm in the right hemisphere. The fact that area V4v, designated as the 'color-sensitive' area in humans by Zeki *et al.* (Zeki *et al.*, 1991), also responded to our random dot stimulus is interesting in itself. For example, in the macaque, area V4 plays a role in both hue and pattern

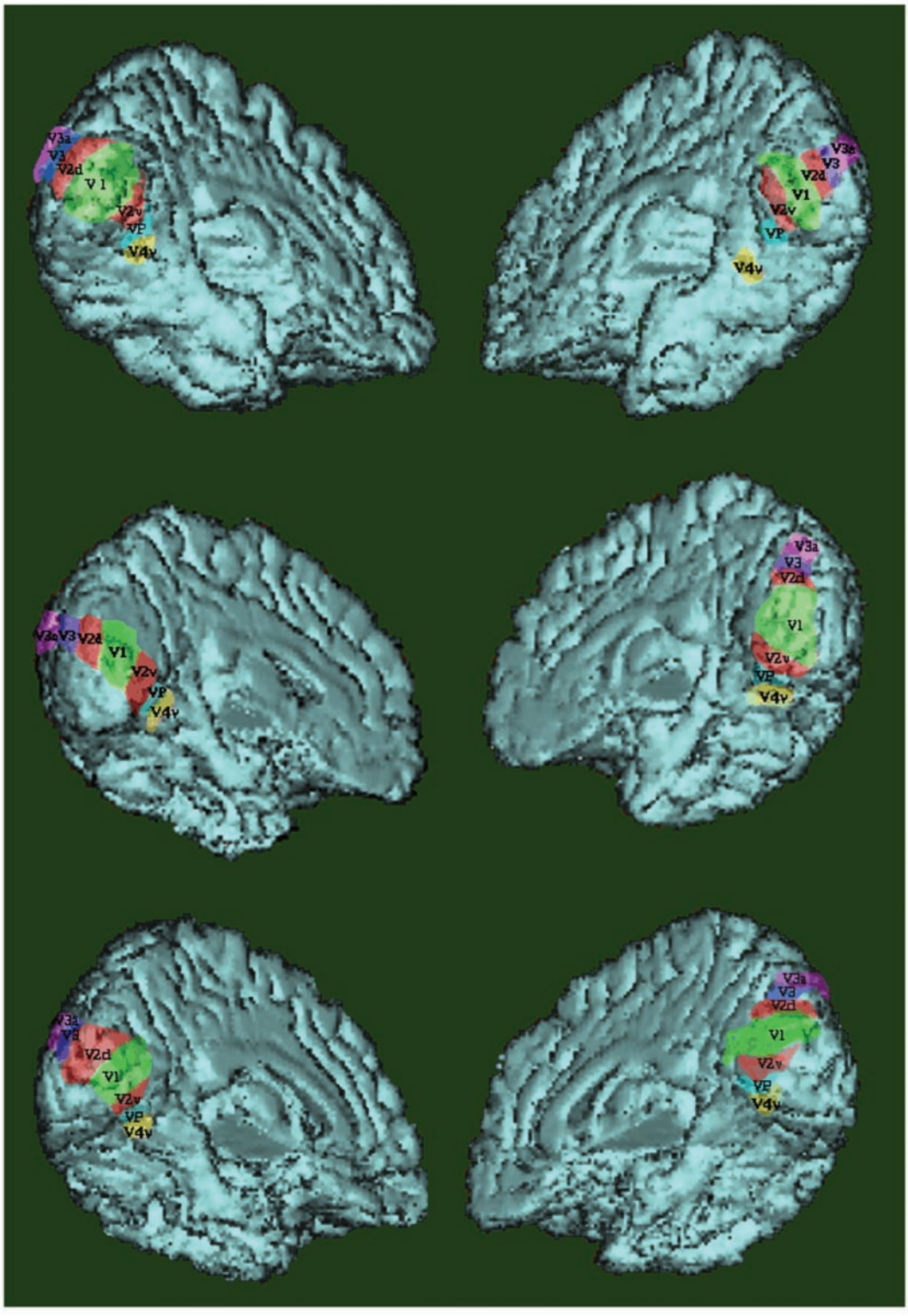

Figure 3. Left and right hemispheres of three subjects illustrating the relative positions of the early visual areas in the occipital lobe. Area locations and shapes are approximate due to the folded sulci of the brain model (e.g. area V4v was usually found inside the folds of the sulcus it is painted on). The resolution of our PET camera was ~5 mm, and the images were interpolated to 8 mm^3 voxel size. The figure is based on the interpolated images.

discrimination (Heywood and Cowey, 1987). When this area is lesioned in macaque, the predominant loss is in form discrimination (Heywood and Cowey, 1993). In humans, Schneider *et al.* reported activations in the fusiform-lingual area (mean Talairach x,y,z coordinates: 23, –11, –74) to a black and white reversing checker-board pattern (Schneider *et al.*, 1993). In agreement with this result, we found activation at this more advanced stage of processing with a relatively simple stimulus.

Table 2
Mean location and standard deviation of the centers of sulci in the medial occipital lobe

Area	Talairach coordinates						Frequency of detection (%)
	Mean location (mm)			Standard deviation (mm)			
	x	*y*	*z*	*x*	*y*	*z*	
Right hemisphere ($n = 11$)							
Calcarine sulcus	7	–78	2	1.8	4.9	5.4	100
Collateral sulcus (posterior limb)	14	–70	–9	2.1	6.6	4.2	91
First dorsal sulcus	5	–86	7	2.3	5.1	5.3	100
Second dorsal sulcus	8	–85	13	3.2	5.0	6.0	100
First ventral sulcus	8	–77	–9	3.2	5.0	6.3	100
Second ventral sulcus	11	–69	–7	3.0	6.8	4.5	100
Cuneosagittal sulcus	2	–82	11	1.3	1.3	5.9	27
Intralingual sulcus	3	–76	–3	2.6	3.5	5.3	27
Left hemisphere ($n = 11$)							
Calcarine sulcus	–7	–81	0	2.2	3.4	5.3	100
Collateral sulcus (posterior limb)	–13	–73	–11	3.4	7.6	4.6	100
First dorsal sulcus	–6	–87	5	2.3	6.7	8.4	100
Second dorsal sulcus	–5	–87	11	1.8	3.0	8.9	100
First ventral sulcus	–8	–79	–12	3.4	4.7	4.6	100
Second ventral sulcus	–11	–71	–9	3.8	5.3	5.1	100
Cuneosagittal sulcus	–3	–78	10	1	3.7	7.9	27
Intralingual sulcus	–6	–76	–4				9

x-axis = medial–lateral axis; positive values indicate location to the right, and negative values location to the left from the midsagittal plane, in millimeters. *y*-axis = anterior–posterior axis; positive values describe location anterior to, and negative values location posterior to the anterior commisure, in millimeters. *z*-axis = superior–inferior axis; positive values are location superior to, and negative values are locations inferior to the bicommisural line connecting the anterior commisure and the posterior commisures, in millimeters.

Sulcal Landmarks

The calcarine sulcus, the first and the second ventral sulci, as well as the first and the second dorsal sulci were found in all 22 hemispheres (Table 2). The posterior limb of the collateral sulcus was identifiable in all 11 left hemispheres and in 10 out of 11 right hemispheres. In the right hemisphere, the posterior limb of the collateral sulcus also happened to be the first ventral sulcus in one individual, and the second ventral sulcus in four individuals. In the left hemisphere, the posterior limb of the collateral sulcus was the same as the first ventral sulcus in three cases, and the same as the second ventral sulcus in six cases. The cuneosagittal sulcus was present as a distinct entity in only three left and three right hemispheres. The intralingual sulcus was present as a distinct entity in only one left and three right hemispheres. Consequently these two sulci were not included in any further analysis

Sulcal Variability

The standard deviations of the sulcal centers were in the same range as the standard deviations of the functional areas for the *y*- and *z*-axes (±5.5 mm). However, the average of standard deviations for the occipital sulci in the *x*-axis (±2.7 mm) was significantly less than the average of standard deviations for functional areas in the *x*-axis (±4.3 mm) ($P < 0.001$). The average of standard deviations for the sulci in the *x*-axis was also significantly less than the average of standard deviations for the sulci in the *y*- and *z*-axes ($P < 0.001$). This was true in both hemispheres. The most likely explanation is the orientation of the sulci being examined (most being parallel to the *x*-axis), and the fact that the sulcal depths of medial occipital sulci (which occur along the *x*-axis) varied from 1 to 4 cm. Thus, the range in which a central point for a sulcus could vary on the *x*-axis was limited to <30 mm. Our findings of asymmetry between the standard deviations of sulcal central points in the three axes mirror those of Thompson *et al.* (Thompson *et al.*, 1996), who found that occipital sulci exhibited greatest variance in the *z*-axis, and reported an even greater degree of asymmetry than encountered in our analysis [a number of other studies have recently investigated sulcal variability (Ono *et al.*, 1990; Steinmetz *et al.*, 1990; Rademacher *et al.*, 1993; Rajkowaska and Goldman-Rakic, 1995; Ide *et al.*, 1996; Paus *et al.*, 1996; Zilles *et al.*, 1997; Leonard *et al.*, 1998; Lohmann *et al.*, 1999)].

Primary Visual Cortex

Right Hemisphere

The geometric center of V1 in the right hemisphere lay closest to the calcarine sulcus in 8 out of 11 subjects (mean distance, d = 7.5 mm). Of the remaining three subjects, two had the geometric center of right V1 over the cuneosagittal sulcus, and one had the geometric center of right V1 over the first ventral sulcus on the medial surface of the occipital lobe. However, in all 11 subjects the calcarine sulcus was included within the boundaries of right V1.

We also compared the location of the contralateral HM representation in right V1 [V1(H)] with that of the calcarine sulcus. Of the 11 individuals in our study, nine had the center of the right V1(H) located within the calcarine sulcus (d = 8.7 mm). In four of these nine individuals right V1(H) was centered in the fundus of the calcarine sulcus. Of the remaining five individuals, four had the right V1(H) activation centered midway between the fundus and the lip of the calcarine, and one had the center of right V1(H) on the dorsal lip of the right calcarine. In six out of nine subjects, the center of right V1(H) was halfway up the length of the calcarine sulcus from the occipital pole. Out of the remaining three subjects, one had the right V1(H) center one-third of the way up the length of the calcarine sulcus, and two had it one-quarter of the way up from the occipital pole. This variance in location was despite the fact that the same HM stimulus out to 18 eccentricity was used in all subjects.

Quite unexpectedly, in two of the 11 individuals the calcarine sulcus was not the closest sulcus to the right V1(H) activation site. In these two individuals, one had right V1(H) centered around the cuneosagittal sulcus, whereas in the other it was

Table 3
Areas and sulci with significant positive correlations in atleast two axes ($P < 0.05$ in each axis)

	Area–sulcal correlations (r)				Area–area correlations (r)			
		x	y	z		x	y	z
Right hemisphere								
V1	V1(H)–second ventral sulcus	0.681	0.734	0.252	V1–V2d	0.316	0.816	0.671
					V1–V2v	0.895	0.945	0.861
					V1–VP	0.733	0.521	0.640
					V1(H)–V2v/VP	0.439	0.705	0.714
V2d	V2d–calcarine	0.246	0.648	0.648	V2d–V3	0.801	0.788	0.782
	V2d–second dorsal sulcus	0.091	0.629	0.706				
V3	V3–calcarine	0.042	0.707	0.718	V2d/V3–V3/V3a	0.717	0.770	0.768
	V3/V3a–calcarine	–0.074	0.724	0.611				
	V3/V3a–second dorsal sulcus	–0.108	0.618	0.657				
V2v	V2v–first ventral sulcus	–0.297	0.657	0.679	V2v–VP	0.768	0.612	0.830
	V2v–second ventral sulcus	0.260	0.755	0.663				
	V2v/VP–second ventral sulcus	0.423	0.828	0.761				
Left hemisphere								
V1	V1–calcarine	0.728	0.855	0.904	V1–V2d	0.761	0.589	0.893
	V1–second dorsal sulcus	0.580	0.741	0.901	V1–V2v	0.499	0.764	0.972
	V1(H)–second dorsal sulcus	0.376	0.828	0.835	V1–V4v	0.629	0.704	–0.342
	V1/V2d–calcarine	0.616	0.875	0.873	V1(H)–V1/V2d	0.750	0.452	0.904
	V1/V2v–calcarine	0.462	0.699	0.797	V1(H)–V2d/V3	0.696	–0.083	0.688
V2d	V2d–calcarine	0.431	0.909	0.816	V2d–V3	0.791	0.783	0.868
	V2d–second ventral sulcus	–0.515	0.692	0.867	V1/V2d–V1/V2v	0.115	0.737	0.783
	V1/V2d–first ventral sulcus	0.608	0.436	0.780				
V3	V3–calcarine	–0.121	0.679	0.698	V2d/V3–V3/V3a	0.741	0.720	0.629
	V3–second ventral sulcus	–0.671	0.639	0.843				
	V2d/V3–second ventral sulcus	–0.542	0.638	0.856				
V2v	V2v–calcarine	0.501	0.833	0.838	V2v–VP	0.085	0.714	0.830
	V2v–second ventral sulcus	0.248	0.697	0.770				
	V1/V2v–second dorsal sulcus	0.446	0.655	0.806				
VP	V2v/VP–first ventral sulcus	0.623	0.439	0.728	V2v/VP–antVP	–0.734	0.686	0.714
	V2v/VP–second ventral sulcus	0.077	0.619	0.816				

Correlation coefficient (r) of 0.6 has a significance of $P < 0.05$ for $n = 11$.

x-axis = medial–lateral axis; y-axis = anterior–posterior axis; z-axis = superior–inferior axis.

centered around the superior extent of the first ventral sulcus. This led to an absence of significant spatial correlation of the right calcarine sulcus with right V1, or with any of the borders of right V1 in any of the axes. The lack of significant spatial covariance was despite the fact that the calcarine was used to help define V1(H), and was the closest sulcus to right V1 in eight out of 11 individuals. The only significant area–sulcal spatial covariance for right V1 occurred between right V1(H) and the second ventral sulcus. Area V1 spatially covaried with area V2d and with area V2v (Table 3). This is as expected because both these areas are adjoining areas. Right V1 also covaried significantly with right VP. Looking closer at this relationship, it was V1(H) representing the contralateral HM that covaried with the contralateral HM representation at the right V2v/VP border. Intriguingly, both these representations also spatially covaried with the second sulcus ventral to the calcarine.

Left Hemisphere

In contrast to the right hemisphere, the calcarine sulcus was the closest sulcal landmark to the geometric center of V1 in the left hemisphere of all 11 subjects (d = 6.4 mm). The center was located within the calcarine sulcus in six individuals, and around the lip of the calcarine sulcus on the medial wall of the occipital lobe in five individuals.

We also compared the location of the left V1(H) to that of the calcarine sulcus in the left hemisphere. Again, in contrast to the right hemisphere, left V1(H) was centered inside the calcarine sulcus in all 11 subjects (d = 6.6 mm). The center of left V1(H) was located midway between the fundus and the lip of the calcarine in seven individuals, whereas four subjects had the center located in the fundus. Starting from the occipital pole, the center of left V1(H) activation was located one-quarter of the way up the length of the calcarine sulcus in two individuals, one-third of the way up in five individuals, one-half of the way up the length of the calcarine in three subjects and two-thirds of the way up the length of the calcarine in one subject.

As a whole, the left primary visual cortex spatially covaried with the calcarine sulcus in all three axes (Table 3). Although the calcarine was used to define the HM activation in V1, V1(H) did not show significant covariance with the left calcarine sulcus except on the z-axis. Most likely, this was due to variance as to where V1(H) activation fell with respect to the length of the calcarine. Nevertheless, the border regions of V1/V2d and V1/V2v did spatially covary with the calcarine sulcus. Instead of covarying with the second ventral sulcus as in the right hemisphere, there was a significant spatial covariance of V1 (H) and left V1 as a whole with the second dorsal sulcus. As in the right hemisphere, left V1 spatially covaried with the adjoining areas left V2d and with left V2v. Left V1 also covaried with left V4v. The dorsal and ventral borders of left V1 spatially covaried with each other, and the central left V1(H) region covaried with the dorsal border of V1, indicating a regular structure within left V1. Left V1(H) spatially covaried with the HM representation at the dorsal left V2d/V3 border, as compared to the right V1(H) covariance with the HM representation at the ventral right V2v/VP border.

Overall, there were more significant spatial covariances between left V1 and corresponding sulci, than between right V1

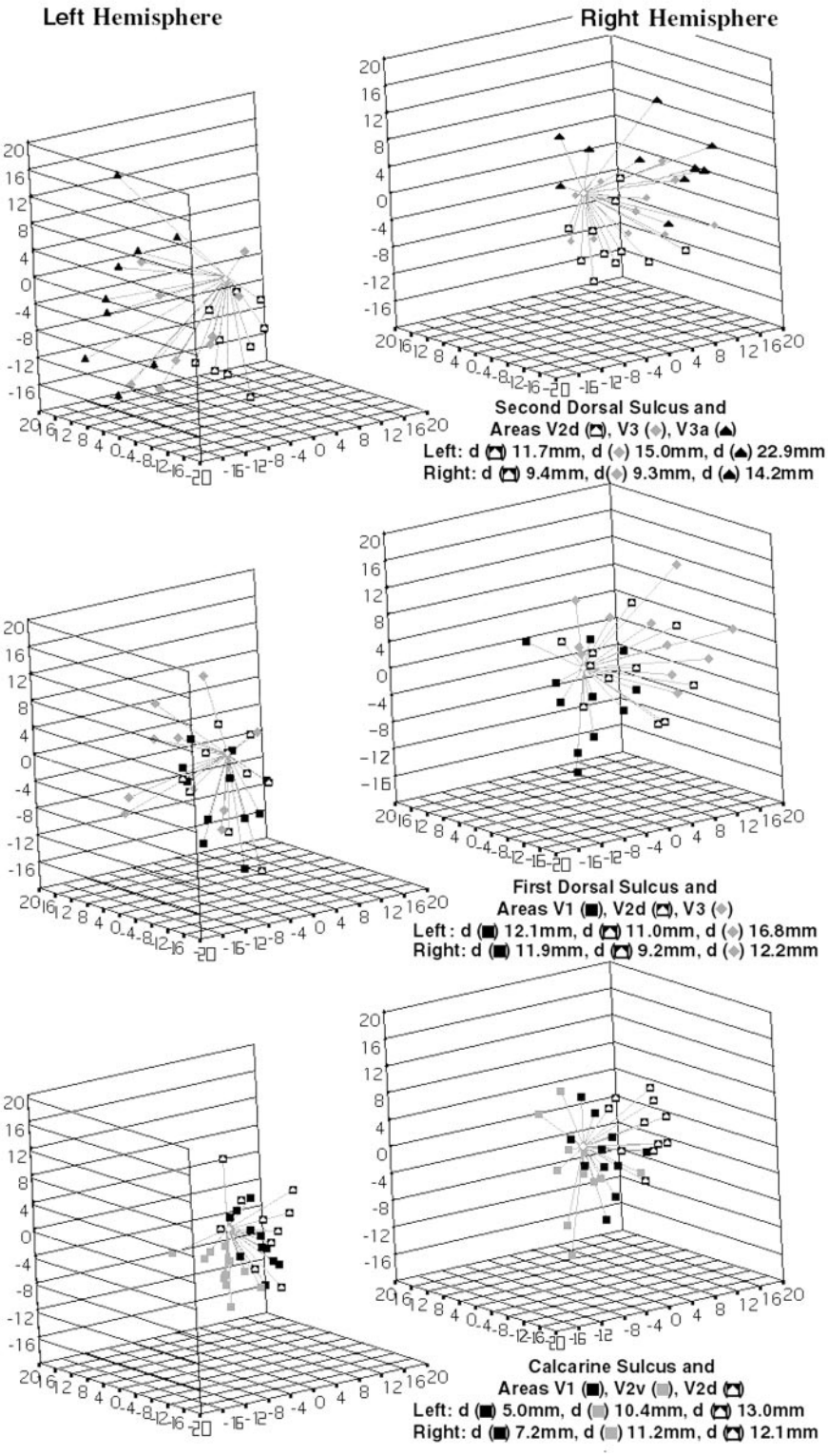

Figure 4. Three-dimensional scatter-plots of neighboring areas around the coregistered centers of the calcarine sulcus and sulci dorsal to the calcarine in eleven subjects. d = mean distance between respective areas and sulci in millimeters, after normalization into Talairach space.

and sulci in the right hemisphere. Right V1 was more variable in terms of its location with respect to the calcarine. There was a bias towards spatial covariance of left V1 with the dorsal sulci and area borders, as compared to covariance of right V1 with the ventral sulci and area borders, in their respective hemispheres.

Areas Dorsal to the Primary Visual Cortex

The first dorsal sulcus was the sulcal landmark closest to the V1/V2d border and to V2d. In more than half the subjects the second dorsal sulcus was the closest sulcus to the V2d/V3 border, area V3, the V3/V3a border and area V3a, across both

hemispheres. The areas and borders dorsal to the primary visual cortex had a tendency to move progressively posterior and superior to the calcarine sulcus such that the V1/V2d border was located dorsal to the calcarine, usually on the exposed surface of the medial occipital lobe (in 18 out of the 22 hemispheres), V2d was located on the medio-posterior curve adjacent to the sagittal sinus, and both V3 and V3a were located on the posterior surface of the occipital lobe (Figs 2 and 3).

Area V2d

Unlike right V1, right V2d spatially covaried with the calcarine sulcus, and with the second dorsal sulcus. There was also spatial covariance with adjoining areas right V1 and right V3. Right V2d/V3 border did not covary with other HM representations at right V1(H) or at the right V2v/VP border.

Area V2d in the left hemisphere was identifiable in 10 out of 11 subjects. Like right V2d, left V2d spatially covaried with the calcarine sulcus in its corresponding hemisphere, and with its adjoining areas left V1 and left V3. It also covaried with the second ventral sulcus. Looking closer, it was the left V2d/V3 border that covaried with the second ventral sulcus. This sulcus had significant spatial covariance with the left V2v/VP border as well (both V2d/V3 and V2v/VP borders represent the contralateral HM). In addition, the HM representation at the left V2d/V3 border significantly covaried with left V1(H). These spatial covariances lend some support to the hypothesis that sulcal formation optimizes axonal distances during morphogenesis.

Area V3

Right V3, like right V2d, significantly covaried with the calcarine sulcus. Looking closer, it was the right V3/V3a border that had significant spatial covariance with the calcarine. The right V3/V3a border also spatially covaried with the second dorsal sulcus (the second dorsal sulcus was most often the closest sulcus to right V3 and right V3a). Moreover, the V3/V3a and V2d/V3 borders of V3 covaried with each other in all three axes, suggesting a regular structure. Significant covariance was found between right V3 and adjoining area V2d, but not with right V3a.

In general, left V3 was found on the posterior surface more often than right V3 (Fig. 3). Left V3, like its right hemisphere counterpart, spatially covaried with the calcarine sulcus, with V2d, and its borders covaried with each other. In addition, left V3 had significant spatial covariance with the second ventral sulcus.

Area V3a

V3a was the last dorsal area that we were able to identify based on the retinotopic organization of the early visual areas. This area was detectable in 10 out of 11 subjects in the right hemisphere. The left V3a was identifiable in nine out of 11 subjects. The border region between V3 and V3a spatially covaried with the calcarine, and with the second dorsal sulcus in the right hemisphere. However, as a whole neither the right V3a nor the left V3a had any significant spatial covariance with any of the sulci. This may be because on average, none of the selected sulci lay within 1.4 cm of V3a (Fig. 4).

Areas Ventral to the Primary Visual Cortex

The visual areas immediately ventral to the primary visual cortex had a tendency to be located progressively inferior and anterior to the calcarine (Fig. 3). The ventral border of V1 with V2v was located inferior to the calcarine sulcus, usually on the exposed surface of the occipital lobe (in 19 out of the 22 hemispheres). When data was pooled together across both hemispheres, the V1/V2v border was closer to the calcarine sulcus than was the V1/V2d border ($P < 0.05$). In contrast to the right hemisphere where the second ventral sulcus tended to be the closest sulcus to area V2v, in the left hemisphere it was the first ventral sulcus that was the closest sulcal landmark to area V2v. Furthermore, the second ventral sulcus was the closest sulcus to the V2v/VP border in the right hemisphere in most subjects, whereas in the left hemisphere there was an equal division of subjects between those with the first ventral sulcus, and those with the second ventral sulcus as the closest sulcal landmark to the V2v/VP border. Thus, there was a tendency for the visual functional areas ventral to the calcarine in the left hemisphere to be closer to the more posterior sulcus, when compared to the right hemisphere (Figs 2 and 3). Both area VP and V4v were closely associated with the posterior limb of the collateral sulcus, such that area VP was usually found at the medial lip, and V4v was found within the posterior limb of the collateral sulcus (in 19 out of 22 hemispheres).

Area V2v

The right V2v spatially covaried with both the first ventral sulcus, and with the second ventral sulcus. It also covaried with adjoining visual area V1, and with area VP. The contralateral HM representation at the right V2v/VP border had significant spatial covariance with the contralateral HM representation in right V1(H). Both V1(H) and the V2v/VP border covaried with the second ventral sulcus. These spatial covariances again suggest that there may be some substance to the hypothesis that sulcal formation optimizes axonal distances during brain development.

There was a tendency for V2v in the left hemisphere to be closer to the more posterior sulcus when compared to the right hemisphere. Like in the right hemisphere, the left V2v spatially covaried with the second ventral sulcus. The left V2v also covaried with the left calcarine sulcus, and with adjoining areas left V1, and left VP. Delving closer into this relationship, it was the left V1/V2v border that spatially covaried with the calcarine sulcus, and the left V2v/VP border that covaried with the second ventral sulcus. Thus, significant spatial covariance was found between the V2v/VP border and the second ventral sulcus in both hemispheres. The left V2v/VP border also covaried with the first ventral sulcus and with the left anterior VP border.

Area VP

In six out of 11 subjects, right VP was located well within the posterior limb of the collateral sulcus, whereas in another individual it was located at the medio-posterior lip of the collateral sulcus. Right VP spatially covaried with right V1 and with right V2v. However, despite a close association with the posterior limb of the collateral sulcus in seven individuals, there was no significant spatial covariance with the center point of the posterior limb of the collateral sulcus.

Like the right hemisphere, left VP was centered well within the collateral sulcus in six out of 11 subjects, and located on the medio-posterior lip of the posterior limb of the collateral sulcus in another. Left VP, like its counterpart in the right hemisphere, spatially covaried with area V2v in its corresponding hemisphere. In addition, the borders of left VP covaried with each other, suggesting a regular structure for the area. As mentioned, the V2v/VP border had significant spatial covariance with the second ventral sulcus in both hemispheres.

Area V4v

Area V4v was identified using the coordinates for the 'color-sensitive' area from Zeki *et al.* as a reference (Zeki *et al.*, 1991). This area was also closely associated with the collateral sulcus. In the right hemisphere, the posterior limb of the collateral sulcus was the closest sulcal landmark in 10 out of 11 subjects (d = 9.7 mm, Fig. 5). The area was located well within the collateral sulcus in these individuals. The left V4v was also closely associated with the collateral sulcus. The area was well within the posterior limb of the collateral sulcus in nine out of 11 subjects (d = 15.1 mm, Fig. 5).

The only significant spatial covariances for area V4v were between left V1 and left V4v. The lack of spatial covariance between area V4v and the posterior limb of the collateral sulcus was surprising, because it was despite the fact that this area was found well within the posterior limb of the collateral sulcus in 10 out of 11 subjects in the right hemisphere, and in nine out of 11 subjects in the left hemisphere. In order to further substantiate this lack of significant spatial covariance, data from both hemispheres were pooled to increase the power of the analysis. The correlation coefficient between the center of area V4v and the center of the posterior limb of the collateral sulcus in the pooled data was 0.048 on the y-axis with a 95% confidence interval of –0.392 to 0.470, and 0.086 in the z-axis with a 95% confidence interval of –0.359 to 0.500. This lack of correlation, reflects that despite an association of area V4v with the posterior limb of the collateral sulcus, there was no strict spatial covariance between the center of area V4v and the center point in the collateral sulcus.

Interhemispheric Covariances

We examined interhemispheric spatial covariances to assess if the location of functional and sulcal landmarks in one hemisphere affected the placement of the corresponding landmarks in the opposite hemisphere during morphogenesis. The left V1, the left V2v and the left calcarine stand out when comparing areas and sulci between hemispheres (Table 4). The left V1 spatially covaried with areas V2d, V2v, V3 and V3a in the right hemisphere. Area V2v in the left hemisphere had significant spatial covariance with right V2v, right VP and right V3. The left calcarine sulcus spatially covaried with the areas right V1, right V2d, right V2v and right V3. This was in contrast to the right calcarine, which covaried only with the right V2d and the right V3, and had no significant spatial correlation with right V1 (Fig. 6).

Discussion

Because sulci not only increase the cortical area but also subdivide the cortex into gyri, a question often posed is whether sulci parcellate the functional map into different areas, i.e. if sulci serve as boundaries for functional areas. Even though this question has not been definitively answered, clinicians routinely use surface anatomy to guide interpretation of lesion locations, and to prognosticate the effects of proposed surgical interventions. Spatial normalization algorithms based on surface landmarks (Van Essen and Drury, 1997) make the same assumption, and lesion-deficit research, such as led by Antonio and Hanna Damasio, is entirely predicated upon this premise (Damasio and Damasio, 1989). Several developmental theories relating sulcation to functional parcellation of the cortex have been put forward, but the hypothesis of sulcal–functional correspondence has only been tested in a qualitative manner. The primary purpose of the present study was to quantify and statistically examine sulcal–function covariance, with both theoretical and practical implications.

Implications for Theories of Sulcation and Gyrogenesis

The Theory of Gyrogenesis

Sanides reported that junctional zones between adjacent micro-anatomical fields run along the beds of major or minor sulci (Sanides, 1962). In their study of sulci in the somatosensory cortex of the family Procyonidae, Welker and Campos observed that sulci reliably predicted boundaries between afferents from different body areas (Welker and Campos, 1963). A functional difference between sulci and gyri was also hinted upon by Preuss and Goldman-Rakic, who found that the crowns of gyri often had a strong contingent of radial myelin fibers in contrast to the sulcal depths, where horizontal fibers predominated (Preuss and Goldman-Rakic, 1991). These reports can best be explained by the theory of gyrogenesis as proposed by Welker (Welker, 1990), which suggests that areas of rapid growth (e.g. the center of a functional zone) will form gyri, so that boundaries between functional areas will tend to lie along sulcal pits. Data in support of this theory come from developing ferret and raccoon brains, showing that the cortices enlarge without the sulcal fundi moving away from the subcortical white matter (Smart and McSherry, 1986) or getting closer to each other.

The Tension-based Theory of Morphogenesis and Compact Wiring

Another theory about sulcation is that sulci form so as to minimize the aggregate axonal distances between strongly connected functional areas (Van Essen *et al.*, 1997). Because early visual areas tend to be retinotopically connected, this means that sulci should form so as to minimize the axonal distances between regions representing the same retinotopic space. For example, because the HM representation in V1 is most often present at the calcarine sulcus, the obvious way to minimize axonal distances between this representation and the HM representations at the V2d/V3 border dorsally, and at the V2v/VP border ventrally, would be for these two borders to be within adjacent sulci.

The Mechanical Hypothesis of Cortical Folding

On the other hand, several investigators have argued that sulcus–function correspondences are generally weak or non-existent. Brodmann (Brodmann, 1909) and more recent studies such as those by Zilles *et al.* (Zilles *et al.*, 1997) found that except in the case of primary sensorimotor cortices, sulci did not reliably mark architectonic boundaries. Moreover, the secondary sulci did not occur predictably. These observations are best explained by the mechanical hypothesis of cortical folding (Richman *et al.*, 1975). According to this hypothesis, the differential growth between the supragranular and granular/infragranular layers causes the cortical surface to buckle under mechanical stress. Thus, sulci should form more or less randomly. Although this hypothesis fails to account for the predictable appearance of the primary sulci, it correctly predicts that microgyria, a condition in which there are numerous shallow gyri, has a greater than normal surface of outer layers as compared to inner layers. Conversely, in lissencephally the surface of outer layers as compared to inner layers is decreased, and the brain surface is relatively smooth with no tertiary gyri. Additional evidence for this hypothesis comes from Zilles *et al.* (Zilles *et al.*, 1989) and Armstrong *et al.* (Armstrong *et al.*, 1991), who observed that in normal rhesus

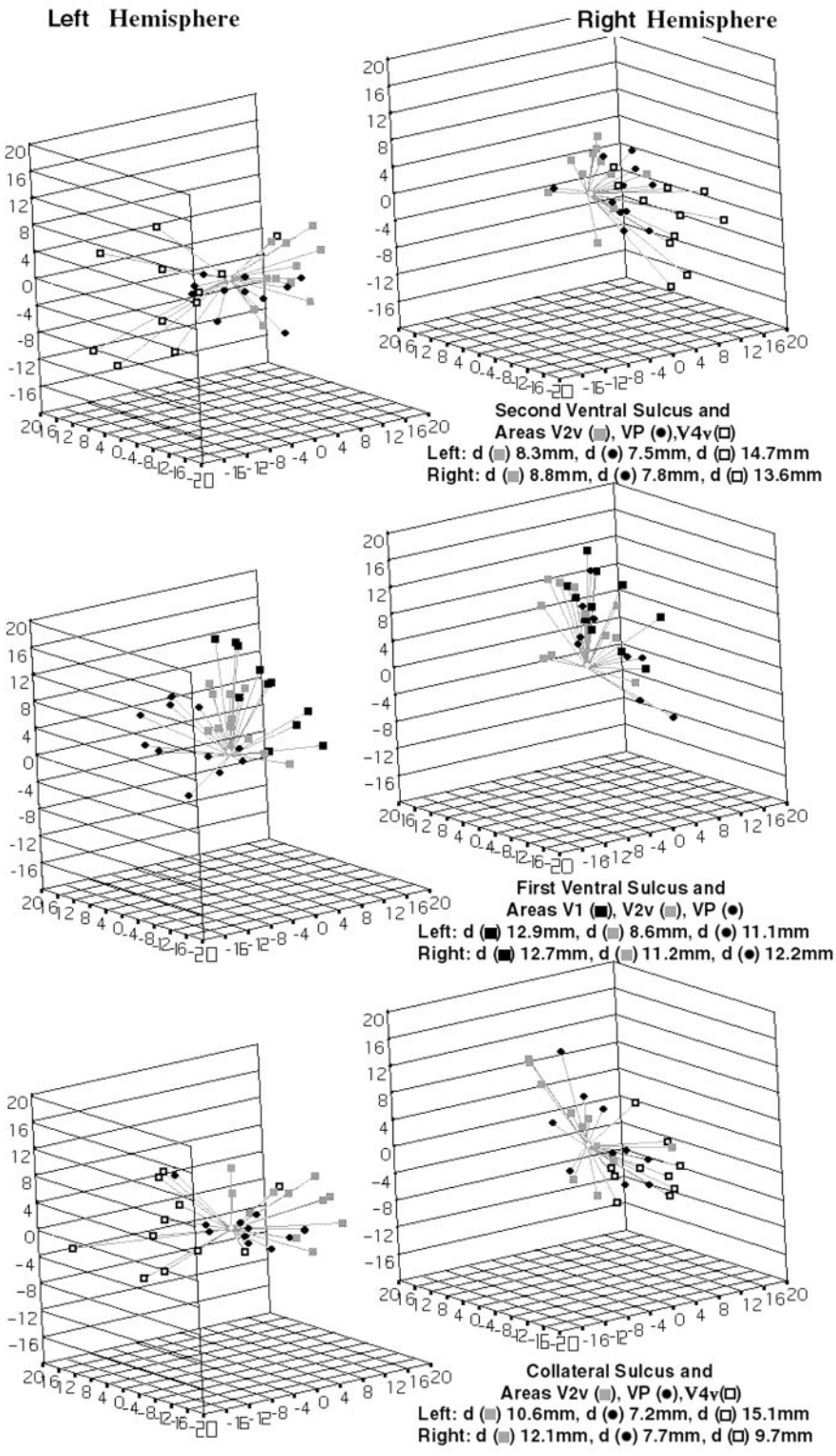

Figure 5. Three-dimensional scatter-plots of neighboring areas around the coregistered centers of sulci ventral to the calcarine, in 11 subjects. Notice the marked asymmetry between left and right hemispheres in the distribution of functional areas around the first ventral sulcus. d = mean distance between areas and sulci in mm, after normalization into Talairach space.

monkeys, both the maximal degree of cortical folding and the maximum surface of outer layers as compared to inner layers occur over the posterior parietal and anterior occipital regions [see papers by Armstrong *et al.* for a discussion on dominant theories of sulcal/gyral development (Armstrong *et al.*, 1991, 1995)].

In our analysis, except for area V4v and the HM representation in V1 (which were usually found within the posterior limb of the

Table 4
Interhemispheric correlations with significance in atleast two axes ($P < 0.05$ in each axis)

	Area–sulcal correlations (*r*)				Area–area correlations (*r*)			
		x	*y*	*z*		*x*	*y*	*z*
Left V1	LV1–right second ventral sulcus	0.477	0.805	0.767	LV1–RV2v	0.015	0.731	0.680
					LV1–RV2d	–0.020	0.916	0.632
					LV1–RV3	–0.007	0.719	0.676
					LV1–RV3a	–0.058	0.633	0.601
Left V2v	LV2v–right second ventral sulcus	0.078	0.731	0.811	LV2v–RV2v	–0.431	0.770	0.685
					LV2v–RVP	–0.206	0.658	0.736
					LV2v-RV3	0.137	0.610	0.666
Left calcarine	RV1–left calcarine	0.477	0.698	0.601				
	RV2v–left calcarine	0.354	0.688	0.682				
	RV2d–left calcarine	–0.201	0.892	0.656				
	RV3–left calcarine	–0.282	0.701	0.655				

Correlation coefficient (*r*) of 0.6 has a significance of $P < 0.05$ for $n = 11$.

x-axis = medial–lateral axis; *y*-axis = anterior–posterior axis; *z*-axis = superior–inferior axis.

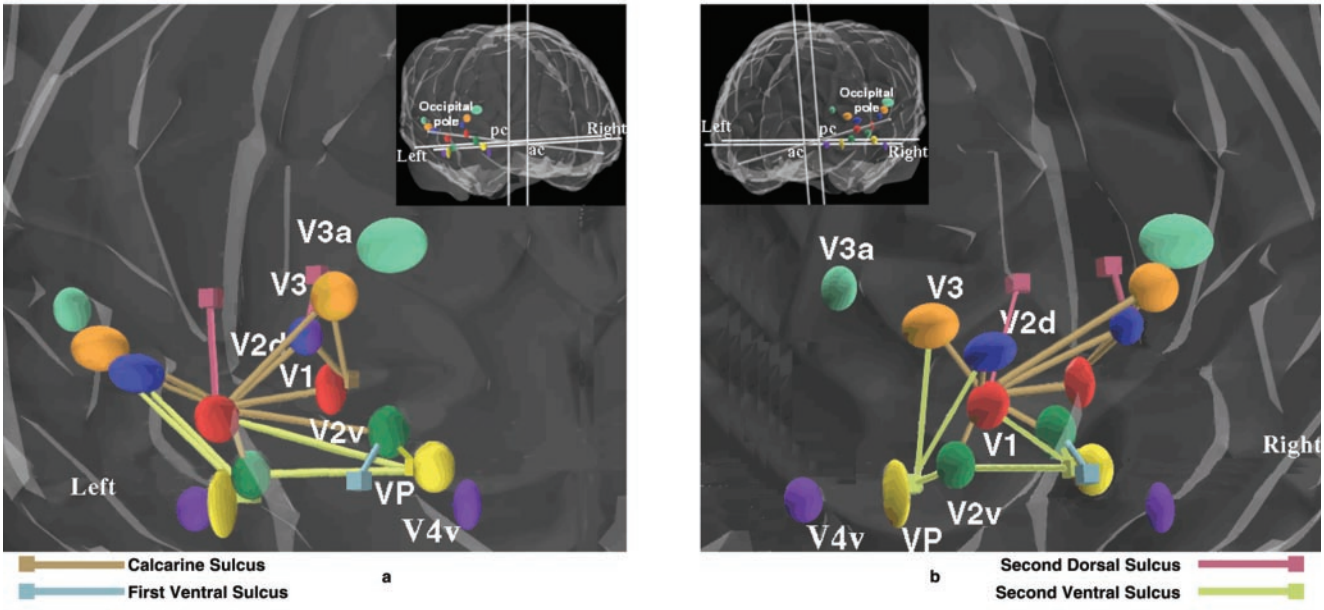

Figure 6. Right posterio-lateral (*a*) and left posterio-lateral (*b*) views of a brain model, illustrating sulcal–functional correlation by lines joining the mean locations of sulcal centers (cubes) with spatially covarying functional areas (ellipsoids) in Talairach space.

collateral sulcus and the calcarine respectively), there did not seem to be any consistent preference of an area or a border to be located within a sulcus or on the exposed surface of the brain. Testing the hypothesis generated by the tension-based theory of morphogenesis and the theory of gyrogenesis, our study found that the V2d/V3 border was located within a sulcus in six out of 11 right hemispheres, and within a sulcus in two out of 10 left hemispheres. The V2v/VP border was located within a sulcus in eight out of 11 right hemispheres, and within a sulcus in six out of 11 left hemispheres. Pooling data across both hemispheres, the HM representation at the V2d/V3 border occurred within a sulcus in only eight out of 21 cases, and the HM representation at the V2v/VP border occurred within a sulcus in 14 out of 22 instances. Similarly, even though the spatial location of the HM representation in area V1 covaried significantly with that at the V2d/V3 border in the left hemisphere, there was no such spatial covariance in the right hemisphere. Conversely, the HM representation in area V1 covaried significantly with that at the V2v/VP border in the right hemisphere, yet the corresponding correlation was absent in the left hemisphere. In brief, although there was some evidence for the hypothesis of minimal axonal distance and the theory of gyrogenesis based on covariance analysis, this evidence remains inconclusive due to a relative dearth of consistent covariances across both hemispheres.

An alternative explanation may be that only one of the HM representations at the V2d/V3 or the V2v/VP borders in a given hemisphere is able to minimize the aggregate axonal distance through sulcation due to the competitive nature of synapse formation (Rakic, 1988). If so, this still does not explain the formation of sulci which did not have either the VM or the HM representations within them. As mentioned above, with the exception of V1(H) and area V4v, there did not seem to be any consistent preference of an area or a border to be located within a particular sulcus or on the exposed surface of the brain. Lack of absolute correspondence between the calcarine and the HM representation in V1 in the right hemisphere is the starkest example of this inconsistency. The considerable variation among subjects in the location of the center-of-activation in V1 with

respect to the length of the calcarine sulcus is another. This lack of strict correspondence has also been reported another group (Aine *et al*., 1996).

In summary, based on our analysis, none of the theories in their present form sufficiently explain the observed selected structure–function covariance, or lack thereof, due to a relative dearth of consistent covariances which were present in both hemispheres between a specific functional area and secondary sulcus. We propose that the timing of formation is more important in determining whether a sulcus will spatially covary with functional architecture, than the overall 'compactness' of the cortical connections. Formation of the primary sulci in mammals occurs during the second trimester, as neurons migrate along glial radials from the ventricular proliferative centers to the cortical surface (Rakic and Singer, 1988). During this stage of radial growth of the cerebral cortex, the development of sulci and functional areas may be tightly linked as witnessed by the relatively constant relationship between primary sulci and functional areas. Thus, the theory of gyrogenesis as proposed by Welker (Welker, 1990), which suggests that areas of rapid growth (e.g. the center of a functional zone) will form gyri, so that boundaries between functional areas will tend to lie along sulcal pits, best explains the linkage at this stage of ontogeny. By the beginning of third trimester the radial neuronal migration is complete. During the third trimester and for some time after birth, the cortical development is predominated by the maturation of the neuropil (Berry, 1982). Moreover, neurons may migrate tangentially at these later stages of corticogenesis (Rakic, 1990). Hence, tangential growth of the cerebral cortex continues after radial migration of neurons is completed. The differential tangent growth of outer cortical lamina when compared with to inner cortical layers as postulated by Richman *et al*. must occur at these later stages because the outer layers are the last to form during radial migration of neurons (Richman *et al*., 1975). Thus, the formation of secondary and tertiary sulci during the third trimester and during the immediate postnatal period may be more influenced by simple mechanical folding of the cortex. This more or less random buckling may actually distort and displace the original placement of the functional areas and would account for the more variable appearance of the secondary and tertiary sulci. In short, sulcal landmarks that form during a period when the radial growth of the cerebral cortex is predominant are more constant and covary with functional areas. On the other hand, sulci that form later during a predominantly tangential growth phase are more variable both in their appearance and in their covariance with functional areas.

Spatial Distribution of Significant Structure–Function Covariances

Although no strict correspondence was present between the boundaries of the early visual areas and the sulcal locations, a certain pattern was present in the distribution of significant sulcal–functional covariances. The majority of functional areas covaried with the calcarine sulcus, the second dorsal and the second ventral sulci (Fig. 6). The only spatial covariances found for the first ventral or the first dorsal sulci were between V2v and the first ventral sulcus in the right hemisphere, and between the V1/V2d and V2v/VP borders and the first ventral sulcus in the left hemisphere. There was a relative abundance of significant area–area as well as area–sulcal spatial covariances in the left hemisphere, when compared to the right hemisphere. Because selected neurons send axons across the corpus callosum even while they are migrating to the cortical surface during morphogenesis (Schwartz *et al*., 1991; Auladell *et al*., 1995), we examined interhemispheric covariances to assess if the location of functional and sulcal landmarks in one hemisphere affected the placement of the corresponding landmarks in the opposite hemisphere. Intriguingly, left V1, left V2v and the left calcarine sulcus covaried significantly with more areas in the contralateral hemisphere than right V1, right V2v and the right calcarine sulcus in their own hemisphere (Table 4). One explanation would be that because the two hemispheres share the confines of the same skull, it is likely that the areas in the two hemispheres will covary. Still, it is hard to explain why the interhemispheric spatial covariances should be more numerous than the intrahemispheric spatial covariances for area V1, area V2v and the calcarine sulcus in the right hemisphere. For example, the left calcarine not only covaried with area V1, area V2v, area V2d and area V3 in its own hemisphere, but also covaried with these same areas in the contralateral hemisphere. These relationships did not hold true for the right calcarine sulcus. Similarly, the left primary visual cortex not only spatially covaried with areas V2v, V2d and V4 in its own hemisphere, but also with area V2v, area V2d, area V3 and area V3a in the contralateral hemisphere (Tables 3 and 4). In contrast, the only significant interhemispheric spatial covariance for the right primary visual cortex was with the left calcarine sulcus. These findings could be explained if right V1 and the right calcarine sulcus were more variable in Talairach space, when compared to their left counterparts. However, the variability of the calcarine and V1 in the two hemispheres was not statistically different in any of the axes (Tables 1 and 2).

Alternatively, one could hypothesize that the primary functional areas and structures in one hemisphere may differentiate before those in the other hemisphere, thus determining dominance and handedness, as well as influencing the placement of functional areas and sulci in the non-dominant hemisphere more strongly than the other way around. Thus, the relative timing of corticogenesis may result in the interhemispheric asymmetry of covariance between sulcal and functional structures, as well as the intrahemispheric pattern present in the distribution of significant sulcal–functional covariances. Interpreted in this manner, the pattern and apparent asymmetry of covariances would support the premise that functional areas and sulci developing early enough during ontogeny will influence the placement of subsequently maturing functional areas.

It was also interesting to note that more significant spatial covariances occurred on the *z*-axis than on any of the other two axes. This may be due to the fact that the sulci and areas in the medio-posterior occipital lobe are organized more or less along the *z*-axis, and can be classified as being ventral (inferior) or dorsal (superior) to the primary visual cortex or the calcarine. In contrast, there were relatively few significant spatial covariances on the *x*-axis, which is more or less perpendicular to the length of the sulci in the medio-posterior occipital lobe. Again, this observation argues that sulcal and functional organizations are interlinked.

Application to Spatial Normalization Algorithms

The practical implications of this study are also notable. The reliability of structure–function relationships is of fundamental importance to pre-operative planning and lesion-deficit research. In addition, spatial normalization is widely used for neuroimaging research, both functional and structural. The great majority of published reports employ linear transformations, which make little or no use of surface anatomy. If

surface anatomy has strong predictive value for functional localization, it could be a valuable addition to present spatial normalization techniques. Ideally, an analysis of structure–function covariance would identify the surface features with the greatest predictive value, for selective incorporation in normalization strategies. Analogously, it has often been suggested that functional areas can serve as landmarks for adjacent functional areas. Many brain-mapping studies, for example, include tasks, which reliably activate well-known areas, to localize new areas by reference. The following are some of the spatial relationships that could be used towards the goal of improving upon linear normalization transforms.

Spatial covariances that were consistent across both hemispheres included significant covariance among adjoining areas, reflecting their common borders. Area V2d and area V3 spatially covaried with the calcarine sulcus in both left and right hemispheres. Also of note was the significant covariance of area V2v and of the HM representation at the V2v/VP border with the second ventral sulcus. These correlations in the inferior occipital lobe were the only notable ones that existed between adjacent sulci and visual areas in both hemispheres. Strong spatial covariance existed between the borders of V3, indicating a regular structure. No other area exhibited this trait across both hemispheres.

If a sulcus and a functional area covary across a population, it follows that, in general, the displacement of one structure from its mean in a particular individual will predict the displacement of the other from its mean in that individual. One method of applying the above findings to better localize an area in a particular individual would be to first identify a sulcus that is known to significantly covary with that area in a particular axis. The second step would be to compute the vector distance between the coordinates for that sulcus and the reported mean coordinates for that sulcus in a stereotaxic space. This vector could then be used to translate the reported mean coordinates for the functional area at issue, thus increasing the probability of localization of the area in that particular individual. For example, the vector distance between the center of the calcarine in a given individual, and the reported mean coordinates for the calcarine on the *y*- and *z*-axes could be calculated. These vectors can then be applied to translate the reported mean coordinates for extra-striate visual areas V2d and V3 on the *y*- and *z*-axes, in order to better localize these areas in that particular individual.

Conversely, this concept can be summarized mathematically by recalling the definition of sample variance:

$$S^2 = \frac{(X_m - X_i)^2}{n-1}$$

If S^2 is the sample variance of a functional area in a stereotaxic space on a particular axis, this variance can be reduced by adding a correctional vector C_i to the mean location X_m for that functional area in each of the individuals based on a sulcus that has been found to covary with that area:

$$S^2 = \frac{\left[(X_m + C_i) - X_i\right]^2}{n-1}$$

In our example, this correctional vector is the displacement of the center of the calcarine in a given subject from the mean coordinates for the calcarine on the *y*- and *z*-axes.

Even though the geometric center of primary visual cortex significantly covaried with the calcarine sulcus in the left hemisphere only, the calcarine was always found to be within the bounds of V1. In addition, area VP and area V4v were closely associated with the posterior limb of the collateral sulcus, such that area VP was usually found at the medial lip of the posterior limb, and area V4v was found within the posterior limb of the collateral sulcus (in 19 out of 22 subjects). These findings can be used to provide limits for a search of these areas in a particular individual.

In summary, the fact that significant spatial correlations between selected sulci and functional areas were obtained suggests that these functional and sulcal landmarks contain information about the structure of the functional map, which is not obviated by nine-parameter normalization. This residual covariance can be used to improve upon the linear normalization algorithms, and may serve as a test for the 'goodness' of spatial normalization techniques.

Notes

We thank S. Mikiten, H. Downs, J. Roby, B. Heyl and P. Jerabek for valuable technical assistance. This study was supported by a grant from the Research Imaging Center and by the Human Brain Project (P20 MH/DA52176).

Address correspondence to Peter T. Fox, MD, Director, Research Imaging Center, The University of Texas Health Science Center at San Antonio, 7703 Floyd Curl Drive, MSC: 6240, San Antonio, TX 78229-3900, USA.

References

Aine CJ, Supek S, George JS, Ranken D, Lewine J, Sanders J, Best E, Tiee W, Flynn ER, Wood CC (1996) Retinotopic organization of human visual cortex: departures from the classical model. Cereb Cortex 6:354–361.

Armstrong E, Curtis M, Buxhoeveden DP, Fregoe C, Zilles K, Casanova MF, McCarthy WF (1991) Cortical gyrification in the Rhesus monkey: a test of the mechanical folding hypothesis. Cereb Cortex 1:426–432.

Armstrong E, Schleicher A, Omran H, Curtis M, Zilles K (1995) The ontogeny of human gyrification. Cereb Cortex. 5:56–63.

Auladell C, Martinez A, Alcantara S, Super H, Soriano E, (1995) Migrating neurons in the developing cerebral cortex of the mouse send callosal axons. Neuroscience 64:1091–1103.

Berry M (1982) Cellular differentiation: development of dendritic arborizations under normal and experimentally altered conditions. Neurosci Res Program Bull 20:451–461.

Brodmann, K (1909) Vergleichende Lokalisationslehre der Grosshirnrinde in ihren Prinzipien dargestellt auf Grund des Zellenbaues. Leipzig: Barth.

Clarke S, Miklossy J (1990) Occipital cortex in man: organization of callosal connections, related myelo- and cytoarchitecture, and putative boundaries of functional visual areas. J Comp Neurol 298:188–214.

Damasio AR, Damasio H (1989) Lesion analysis and neuropsychology. Oxford: Oxford University Press.

Daniel PM, Whitteridge D (1961) The representation of the visual field on the cerebral cortex in monkeys. J Physiol 159:203–221.

Duvernoy H (1991) The human brain. Springer-Verlag: Wien.

DeYoe EA, Carman GJ, Bandettini P, Glickman S, Wieser J, Cox R, Miller D, Neitz J (1996) Mapping striate and extrastriate visual areas in human cerebral cortex. Proc Natl Acad Sci USA 93:2382–2386.

Felleman DJ, Van Essen DC (1991) Distributed hierarchical processing in primate cerebral cortex. Cereb Cortex 1: 1–47.

Fox PT, Raichle ME (1984) Stimulus rate dependence of regional cerebral blood flow in human striate cortex, demonstrated by positron emission tomography. J Neurophysiol 51:1109–1120.

Fox PT, Mintun MA (1989) Non-invasive functional brain mapping by change-distribution analysis of averaged PET images of H_2O^{15} tissue activity. J Nucl Med 30:141–149.

Fox PT, Pardo JV (1991) Does intersubject variability in cortical functional organization increase with neural 'distance' from the periphery? Ciba Foundation Symp 163:125–144.

Fox PT, Mintun MA, Raichle ME, Herscovitch P (1984) A noninvasive approach to quantitative functional brain mapping with H_2O^{15} and positron emission tomography. J Cereb Blood Flow Metab 4:329–333.

Fox PT, Mintun MA, Raichle ME, Miezin FM, Allman JM, Van Essen DC

(1986) Mapping human visual cortex with positron emission tomography. Nature 323:806- 809.
Fox PT, Mintun MA, Reiman EM, Raichle ME (1988) Enhanced detection of focal brain responses using inter-subject averaging and change-distribution analysis of subtracted PET images. J Cereb Blood Flow Metab 8:642–53.
Gattass R, Sousa APB, Gross CG, (1988) Visuotopic organization and extent of V3 and V4 of the macaque. J Neurosci 8:1831–1845.
Hasnain MK, Fox PT, Woldorff MG (1998) Intersubject variability of functional areas in the human visual cortex. Hum Brain Map 6:301–315.
Herscovitch P, Markham J, Raichle ME (1983) Brain blood flow measured with intravenous H_2^{15} O: I. Theory and error analysis. J Nucl Med 24:782–789.
Heywood CA, Cowey A (1987) On the role of cortical area V4 in the discrimination of hue and pattern in macaque monkeys. J Neurosci 7:2601–2617.
Heywood CA, Cowey A (1993) Color and face perception in man and monkey: the missing link. In: Functional organization of the human visual cortex (Gulyas B, Ottoson D, Roland PE, eds), Wenner–Gren International Series Vol. 61, pp. 195–210. Oxford: Pergamon Press.
Holmes G (1945) The organization of the visual cortex in man. Proc R Soc Lond Series B Biol 132:348–361.
Horton JC, Hoyt WF (1991a) The representation of the visual field in human striate cortex. A revision of the classic Holmes map. Arch Ophthalmol 109:816–824.
Horton JC, Hoyt WF (1991b) Quadrantic visual field defects; a hallmark of lesions in the extrastriate (V2/V3) cortex. Brain 114:1703–1718.
Hunton DL, Miezin FM, Buckner RL, van Mier HI, Raichle ME, Petersen SE (1996) An assessment of functional–anatomical variability in neuro-imaging studies. Hum Brain Map 4:122–139.
Ide A, Rodriguez E, Zaidel E, Aboitiz F (1996) Bifurcation patterns in the human sylvian fissure: hemispheric and sex differences. Cereb Cortex 6:717–725.
Lahti BP (1965) Signals, systems and communication, pp. 437–441. New York: Wiley.
Lancaster JL, Glass TG, Lankipalli BR, Downs JH, Mayberg H, Fox PT (1995) A modality-independent approach to spatial normalization of tomographic images of , the human brain. Hum Brain Map 3:209–223.
Leonard CM, Puranik C, Kuldau JM, Lombardino LJ (1998) Normal variation in the frequency and location of human auditory cortex landmarks. Heschl's gyrus: where is it? Cereb Cortex 8:397–406.
Lohmann G, Cramon DYV, Steinmetz H (1999) Sulcal variability of twins. Cereb Cortex 9:754–763.
Mintun MA, Fox PT, Raichle ME (1989) A highly accurate method of localizing regions of neuronal activity in the human brain with PET. J Cereb Blood Flow Metab 9:96–103.
Newsome WT, Maunsel JHR, Van Essen DC (1986) Ventral posterior visual area of the macaque: visual topography and areal boundaries. J Comp Neurol 252:139–153.
Ono M, Kubik S, Abernathy CD (1990) Atlas of the cerebral sulci. Stuttgart: Thieme.
Paus T, Tomaiuolo F, Otaky N, MacDonald D, Petrides M, Atlas J, Morris R, Evans AC (1996) Human cingulate and paracingulate sulci: pattern, variability, asymmetry, and probabilistic map. Cereb. Cortex 6:207–214.
Preuss, TM, Goldman-Rakic, PS (1991) Myelo- and cytoarchitecture of the granular frontal cortex and surrounding regions in the strepsirhine primate Galago and the anthropoid primate Macaca. J. Comp Neurol 310:429–474.
Rademacher J, Caviness VS, Jr, Steinmetz H, Galaburda AM (1993) Topographical variation of the human primary cortices: implications for neuroimaging, brain mapping, and neurobiology. Cereb Cortex 3:313–329.
Raichle ME (1987) Circulatory and metabolic correlates of brain function in normal humans. In: Handbook of physiology – the nervous system, vol. V. pp. 643–674. Washington, DC: American Physiological Society.
Raichle ME, Martin WRW, Herscovitch P, Mintun MA, Markham J (1983) Brain blood flow measured with intravenous H_2 ^{15}O. II. Implementation and validation. J Nucl Med 24:790–798.
Rajkowska G, Goldman-Rakic P (1995) Cytoarchitectonic definition of pre-frontal areas in the normal human cortex. II. Variability in locations of areas 9 and 46 and relationship to the Talairach coordinate system. Cereb Cortex 5:323–337.
Rakic P (1990) Principles of neural cell migration. Experientia 46:882–891.
Rakic P, Singer W. (ed.) (1988) Neurobiology of neocortex, Dahlem Workshop Reports; Life Sciences Research Report 42. New York: Wiley.
Richman DP, Stewart RM, Hutchinson JW, Caviness VS, Jr (1975) Mechanical model of brain convolutional development. Science 189:18–21.
Sanides, F (1962) Die Architektonic des menschlichen Stirnhirns. In: Monographien aus dem Gesamtegebiete der Neurologie und Psychiatrie (Mueller M, Spatz H, Vogel P, eds). Berlin: Springer-Verlag.
Schneider W, Casey BJ, Noll D (1993) Functional MRI mapping of stimulus rate effects, across visual processing stages. Hum Brian Map 1:117–133.
Schwartz ML, Rakic P, Goldman-Rakic PS (1991) Early phenotype expression of cortical neurons: evidence that a subclass of migrating neurons have callosal axons. Proc Natl Acad Sci USA 88:1354–1358.
Sereno MI, Dale AM, Reppas JB, Kwong KK, Belliveau JW, Brady TJ, Rosen BR, Tootell RBH (1995) Borders of multiple visual areas in humans revealed by functional magnetic resonance imaging. Science 268:889–893.
Smart IHM, McSherry GM (1986) Gyrus formation in the cerebral cortex of the ferret. II. Description of the internal histological changes. J Anat 147:27–43.
Steinmetz H, Furst G, Freund HJ (1990) Variation of perisylvian and calcarine anatomic landmarks within stereotaxic proportional coordinates. Am J Neuroradiol 11: 1123–1130
Talairach J, Tournoux P (1988) Principe et technique des etudes anatomiques. In: Co-planar stereotaxic atlas of the human brain 3-dimensional proportional system: an approach to cerebral imaging (Rayport M, ed.), vol. 3, New York: Thieme.
Thompson PM, Schwartz C, Lin RT, Khan AA, Toga AW (1996) Three dimensional statistical analysis of sulcal variability in the human brain. J Neurosci 16:4261–4274.
Van Essen DC (1997) A tension-based theory of morphogenesis and compact wiring in the central nervous system. Nature 23; 385 (6614): 313–318.
Van Essen DC, Zeki SM (1978) The topographic organization of rhesus monkey prestriate cortex. J Physiol 277:193–226.
Van Essen DC, Drury HA (1997) Structural and functional analysis of human cerebral cortex using a surface based atlas. J Neurosci 17:7079–7102.
Welker W (1990) Why does cerebral cortex fissure and fold? A review of determinants of gyri and sulci. In: Cerebral cortex, Vol. 8B (Jones EG, Peters A), pp. 3–136. New York: Plenum.
Welker WI, Campos GB (1963) Physiological significance of sulci in somatic sensory cortex in mammals of the family Procyoniclae. J Comp Neurol 120:19–36.
Woods RP, Mazziota JC, Cherry SR (1993) MRI–PET registration with automated algorithm. , J Comput Assist Tomogr 17:536–546.
Zeki SM, Watson JD, Lueke CJ, Friston KJ, Kennard C, Frackowiak RSJ (1991) A direct demonstration of functional specialization in human visual cortex. J Neurosci 11:641–649.
Zilles K, Armstrong E, Moser KH, Schleicher A, Stephen H (1989) Gyrification in the cerebral cortex of primates. Brain Behav Evol. 34:143–150.
Zilles K, Schleicher A, Langemann C, Amunts K, Morosan P, Palomero-Gallagher N, Schormann T, Mohlberg H, Burgel U, Steinmetz H, Schlaug G, Roland PE (1997) Quantitative analysis of sulci in the human cerebral cortex: development, regional heterogeneity, gender difference, asymmetry, intersubject variability and cortical architecture. Hum Brain Map 5:218–221.